RSC Advances

PAPER

View Article Online
View Journal | View Issue

Cite this: *RSC Adv.*, 2025, **15**, 22128

Effect of solvent composition on a one-dimensional $(NH_4)_2V_{10}O_{25}\cdot 8H_2O$ electroactive material for electrochemical hydrogen storage application

Poria Gomrokchi,[a] Maryam Ghiyasiyan-Arani,*[a] Elmuez A. Dawi,[b] Forat H. Alsultany,[b] Salman Khalaf Issa,[cd] Mehdi Shabani-Nooshabadi[a] and Masoud Salavati-Niasari*[a]

Received 1st May 2025
Accepted 10th June 2025

DOI: 10.1039/d5ra03066h

rsc.li/rsc-advances

Electrode materials with tailored shapes for one-dimensional (ID) nanorods were manufactured using a solvothermal approach. Different conditions led to the formation of samples with diverse morphologies and compositions. Structural characteristics were studied using XRD, FT-IR, EDX, FE-SEM, TEM and BET analysis $(NH_4)_2V_6O_{16}$ and $(NH_4)_2V_{10}O_{25}\cdot 8H_2O$ structures were obtained under these conditions. The charge–discharge test was conducted to compare the activity of electrode materials with different phase purities. After 15 cycles at a current density of 1 mA, the fabricated $(NH_4)_2V_{10}O_{25}\cdot 8H_2O$ material displayed a capacity of 956 mA h g^{-1}, and a maximum capacity of 5268 mA h g^{-1} was obtained at the 7th cycle. However, the $(NH_4)_2V_6O_{16}$ electrode material showed 324 mA h g^{-1} capacity. Vanadium-based materials have poor conductivity. Therefore, designing 1D structures improves the hydrogen storage efficiency of the electrodes. The optimized sample with a nanorod structure and $(NH_4)_2V_{10}O_{25}\cdot 8H_2O$ phase purity shows a surface area of 23.571 m^2 g^{-1}.

1. Introduction

One of the most important issues around the world is related to energy, which can be produced from renewable or non-renewable sources. For example, oil is the only energy source on which 95% of transportation systems depend. Most of the world's energy comes from fossil fuels, raising two issues, namely, the depletion of fossil fuels and their exhaustion as well as the discharge of greenhouse gases, which cause global warming and air pollution.[1]

Therefore, scientists are looking for alternative and clean fuels. Consequently, hydrogen has been introduced into the market, which is an eternal and clean energy, environment-friendly, abundant, and non-toxic; moreover, its combustion does not emit greenhouse gases.[2,3] Hydrogen has three times the chemical energy of some fossil and chemical fuels (143 MJ per kg). Burning fossil fuels releases molecular hydrogen and carbon dioxide into the atmosphere, thereby increasing pollution, whereas the only product of the hydrogen and oxygen evolution reaction is gaseous water vapor.[4–6]

Hydrogen can be produced from wind energy,[7] solar energy,[8] geothermal energy,[9] natural gas, coal or oil,[10] and biomass.[11] Hydrogen storage is divided into three ways: (i) compressed hydrogen storage, which has two drawbacks. This method causes high diffusivity and hydrogen embrittlement problems because high-strength steel and a high-weight tank are required. Therefore, it is important to pay attention to safety procedures.[12,13] (ii) Liquid hydrogen storage: the process of storing liquid hydrogen not only requires a significant amount of energy, but also results in substantial hydrogen loss due to its boiling.[14] (iii) Solid-state storage: in this method, hydrogen can be stored physically or chemically.

Physisorption allows hydrogen to easily adsorb and desorb from high-surface manufactured materials. Hydrogen is adsorbed *via* weak van der Waals interactions during physisorption. Physical adsorption can occur in porous materials with high-carbon structures, carbon nanotubes, metal organic frameworks, zeolites, and other recently developed intrinsically porous polymers.[15] Chemisorption occurs when hydrogen dissociates into two atoms and forms chemical bonds with synthetic materials. Hydrogen can be released through heat disintegration, but this type of adsorption is irreversible. Chemical adsorption occurs in metal hydrides, complex

[a]*Institute of Nano Science and Nano Technology, University of Kashan, Kashan 87317-51167, Islamic Republic of Iran. E-mail: m.ghiyasiyan@kashanu.ac.ir; salavati@Kashanu.ac.ir; Fax: +98 31 55913201; Tel: +98 31 55912383*

[b]*College of Humanities and Sciences, Department of Mathematics and Sciences, Ajman University, P. O. Box 346, Ajman, United Arab Emirates*

[c]*Department of Medical Physics, College of Sciences, Al-Mustaqbal University, Babylon, 51001, Iraq*

[d]*Department of Medical Laboratories Technology, Al-Nisour University College, Nisour Seq. Karkh, Baghdad, Iraq*

hydrides, amides, imides, mixtures, and clathrate hydrates.[1] Therefore, selecting suitable materials for hydrogen sorption is an essential task. Metal oxides are a large category of hydrogen sorption materials because of their stability, accessibility, and easy synthesis methods.

In the past few years, vanadate and poly-vanadate have been mentioned as highly promising electrode materials in energy devices because of their high abundance and mixed oxidation states of vanadium (V^{5+} to V^{3+}), high theoretical specific capacity, which goes back to its layer structure with adjustable tunnels structure and property of being non-toxic.[16–19] NH_4VO_3 was used as a vanadium-based source. It has several advantages, such as being cheap. In terms of quantity, it is more readily available than lithium and several redox reactions. The stability of the structure is caused by the hydrogen bonds between NH_4^+ and the VO layer; in addition, it plays an important role in the enforcement of long-cycling stability.[20,21] In the previous literature, the $(NH_4)_2V_{10}O_{25}\cdot 8H_2O$ was synthesized by Hanmei Jiang *et al.* using a facile hydrothermal method and reported as a cathode material for high-performance aqueous zinc-ion batteries. Thus, the synthesized Zn//$(NH_4)_2V_{10}O_{25}\cdot 8H_2O$ nanobelts showed capacities as high as 417, 366, 322, 268 and 209 mA h g^{-1} at 0.1, 0.2, 0.5, 1.0 and 2.0 A g^{-1}, respectively. In addition, the synthesized material has an energy density of 320 Wh kg^{-1} and good cycle ability after 100 cycles.[22] In another work, Yingchang Jiang *et al.* reported the synthesis of $(NH_4)_2V_{10}O_{25}\cdot 8H_2O$ by a hydrothermal method and the morphology of urchin-like hierarchical arrays as superior electrodes for all-solid-state supercapacitors. The reported results deliver a specific capacitance of 1530 F g^{-1} at a current density of 1.5 A g^{-1} and retain 95.1% of the initial capacitance after 10 000 cycles.[23] Tongye Wei *et al.* synthesized ultrathin $(NH_4)_2V_{10}O_{25}\cdot 8H_2O$ nanobelts by a hydrothermal method and used them as a new feasible cathode material for rechargeable zinc-ion batteries. It shows long cycling stability of more than 90.1% after 5000 cycles at a high current density of 5 A g^{-1}.[24] The designed composites based on $(NH_4)_2V_6O_{16}\cdot 1.35H_2O$@graphene oxide @carbon nanotube as the cathode attain a 305 mA h g^{-1} capacity and have stability during 10 000 cycles. In addition, the application of $(NH_4)_2V_6O_{16}\cdot 1.35H_2O$@graphene oxide@carbon nanotubes was investigated in a Ca-ion hybrid capacitor full cell that provides a capacity of 62.8 mA h g^{-1}.[25] Vanadium-based materials are environmentally friendly, safe, and abundant in the earth's crust (300 times more than lithium), have numerous redox processes, are cheap cost, and have layered structures with programmable tunnels.[26] The VO layers, interstitial NH_4^+, and H_2O are more stable because of the hydrogen bonds (N–H/O) between them. This cohesiveness improvement reduces structural changes during the charge/discharge cycle. It is essential for long-term stability.[27]

Nanomaterials' huge surface area, great electrical conductivity, and short diffusion paths improve electrochemical performance and energy capacity. Electrochemical techniques can be used to manufacture nanostructured electrode materials such as metal oxides, carbon-based materials, and metal nanocomposites. These materials have good topologies and interfaces for charge transport and storage. The behavior and performance of nanoparticle-based devices can be described in different interesting aspects. The size, structure, and interface may inspire these features. Nanotechnology characterizes materials with more surface area as zero-dimensional, one-dimensional, or two-dimensional. Scientists are building nanostructures to improve electrode performance. Electrode modifiers include nanotubes, nanoparticles, and nanowires.[28,29] To provide good electroactive sites and quick electron/ion transit, vanadate nanoparticles must be designed to increase electrochemical performance because of their low proficiency and electrochemical stability. Designing 1D nanostructures enhances the performance of vanadium-based electrode materials.[30]

In this study, $(NH_4)_2V_{10}O_{25}\cdot 8H_2O$ with a uniform 1D nanorod morphology was synthesized by a facile solvothermal method. In this work, different solvent mixtures were investigated. In the next step, these synthesized materials are used as electroactive materials in hydrogen storage. In the following, the chrono-potentiometric method was used to determine the hydrogen storage capacity of different samples.

2. Experimental section

2.1. Material

The chemical precursors and starting materials used in the synthesis process of samples, including ammonium vanadate (≥99.0%), oxalic acid (98%), and 2-propanol, were purchased from Merck company and used as received without further purification.

2.2. Synthesis

To fabricate ammonium vanadium oxide structures, 0.58 g NH_4VO_3 and 1 g of oxalic acid were dissolved in the specified solvent and mixed in a beaker under a heater stirrer for 3 hours to form an orange solution. The obtained orange solution was transferred to an autoclave and placed in an oven for 24 hours at 120 °C. After cooling the reaction autoclave, a dark green precipitate was obtained, which was separated from the solution using a centrifuge. The washed precipitate was dried in an oven at a temperature of 80 °C (Scheme 1). The effects of solvent mixtures on product purity and morphology were investigated by selecting different propanol/water ratios. Samples NHV1, NHV2 and NHV3 were provided in the propanol/water solvent at ratios of 40 : 60, 20 : 80 and 10 : 90, respectively. The fabricated sample in the presence of 100% water is denoted as NHV0.

2.3. Electrochemical section

Each sample's hydrogen storage capacity and electrochemical characteristics were measured using chronopotentiometry in a three-electrode cell. The cell consisted of a functioning Pt counter and Ag/AgCl reference electrodes. The electrolyte was 2.0 M KOH. The working electrode was made by placing a thin layer of the as-synthesized powder samples on a pure copper plate substrate. This was achieved by dispersing the as-synthesized nanostructures in ethanol and subjecting the

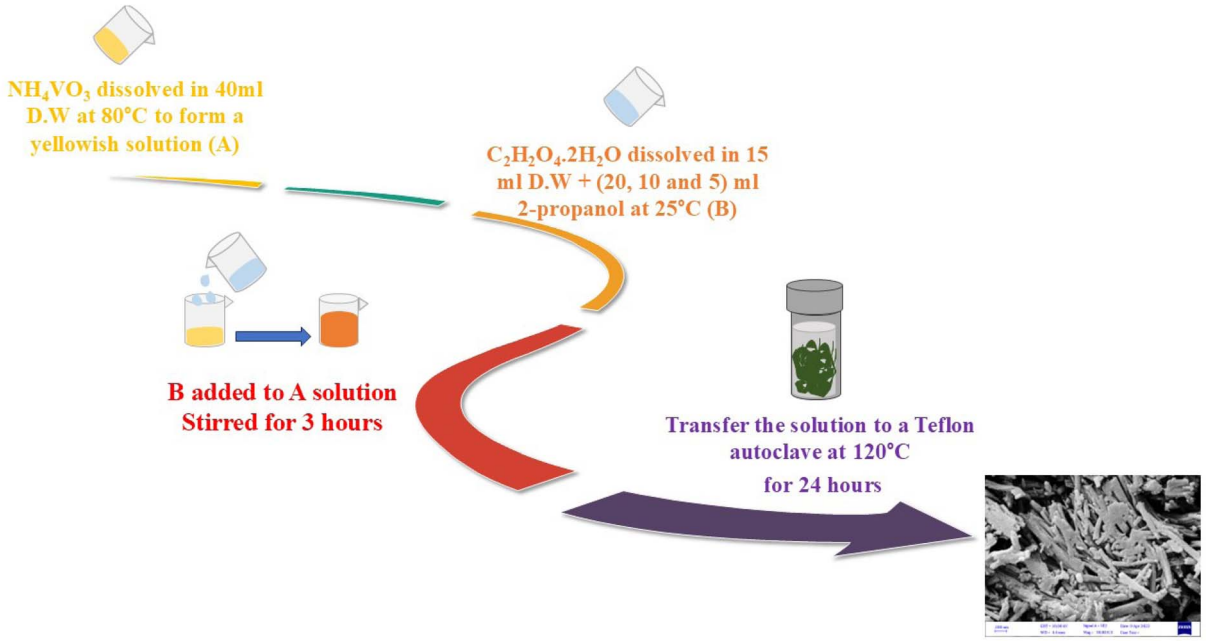

Scheme 1 Synthesis of NHV samples through a step-by-step solvothermal method.

mixture to ultrasonic treatment for 15 min to obtain a homogenous coating solution. The solution was then pipetted onto a copper substrate and dried at 80 °C without a binder to form a thin coating. An ambient electrochemical cell was created. By transmitting a constant current between the working and counter electrodes, the working electrode potential was measured against the reference electrode.

3. Results

3.1. Structural characterization

The fabricated samples in the different solvent mixtures were studied in terms of their purity and crystal phase characteristics, as shown in Fig. 1a–d. Sample NHV0 (Fig. 1a), which was synthesized as a blank sample in D.I. water, matched the reference pattern of 26-0097 related to the $(NH_4)_2V_{10}O_{25}\cdot 8H_2O$. Also, samples NHV1 (Fig. 1b) and NHV3 (Fig. 1d) displayed the same XRD pattern with phase purity of $(NH_4)_2V_{10}O_{25}\cdot 8H_2O$. However, sample NHV2 (Fig. 1c) exhibited sharp peaks, confirming the preparation of $(NH_4)_2V_6O_{16}$ (JCPDS = 79-2051). The crystal structure of each sample was investigated in terms of microstrain and grain size, which was calculated using Williamson–Hall and Scherrer methods. The grain sizes of samples NHV0, NHV1, NHV2 and NHV3, calculated using the Scherrer formula, were 15.8, 12, 32.6 and 24.6 nm, respectively. On the other hand, grain size can be studied using the Williamson–Hall plot, as shown in Fig. 2. According to the Williamson–Hall plot, by plotting $\beta \cos\theta$ *versus* $\sin\theta$, the grain size is equal to $K\lambda$/intercept, and the microstrain is related to the slope of each plot. Therefore, the grain sizes obtained using the Williamson–Hall method for samples NHV0, NHV1, NHV2 and NHV3 were 16.9, 8.2, 40.7, and 34.6 nm, respectively.

Chemical bands for ammonium vanadate samples NHV1, NHV2 and NHV3 are shown in the FT-IR spectra (Fig. 3(a–c)). The bands appearing around 1000,734 and 537 cm^{-1} are related to V–O–V, V–O and V=O, respectively, from the VO negative layer.[31,32] The vibrations at 1406 cm^{-1} and 3188 cm^{-1} are assigned to the in-plane stretch vibration of the N–H bond of NH_4^+ between the VO layers.[22] Two vibrations that appeared at about 1616 cm^{-1} and 3413 cm^{-1} indicated the existence of water on the surface of the product.[33] Fig. 4(a–c) separates the elemental purity of samples NHV1, NHV2, and NHV3. All EDS results from the demonstration presence of N, V, and O without any impurities.

The morphology and size of fabricated samples in a medium containing different solvent mixtures were investigated using FE-SEM, as shown in Fig. 5. Fig. 5(a and b) shows the FE-SEM images of sample NHV1 and presents large structures that are agglomerated. Fig. 5(c and d) illustrates the morphology of sample NHV2, which contains agglomerated sheets. However, sample NHV3 (Fig. 5(e and f)) expressions for nanorods of $(NH_4)_2V_{10}O_{25}\cdot 8H_2O$ with a diameter of 40–80 nm.

According to the above characterization in terms of purity and morphology, NHV2, which was synthesized in the presence of 20% propanol, exhibited different purities ($(NH_4)_2V_6O_{16}$) and morphologies. Correspondingly, the $(NH_4)_2V_{10}O_{25}\cdot 8H_2O$ sample shows optimized morphology in the presence of 10% propanol in the synthesis solvent.

Detailed information about the structure of the fabricated $(NH_4)_2V_{10}O_{25}\cdot 8H_2O$ sample was obtained from the TEM images at different magnifications. Fig. 6(a–c) displays nanorods of $(NH_4)_2V_{10}O_{25}\cdot 8H_2O$ structures.

The internal pressure increased because of solvent vaporization during solvothermal synthesis in a sealed autoclave. Solvents with lower boiling points have a higher internal

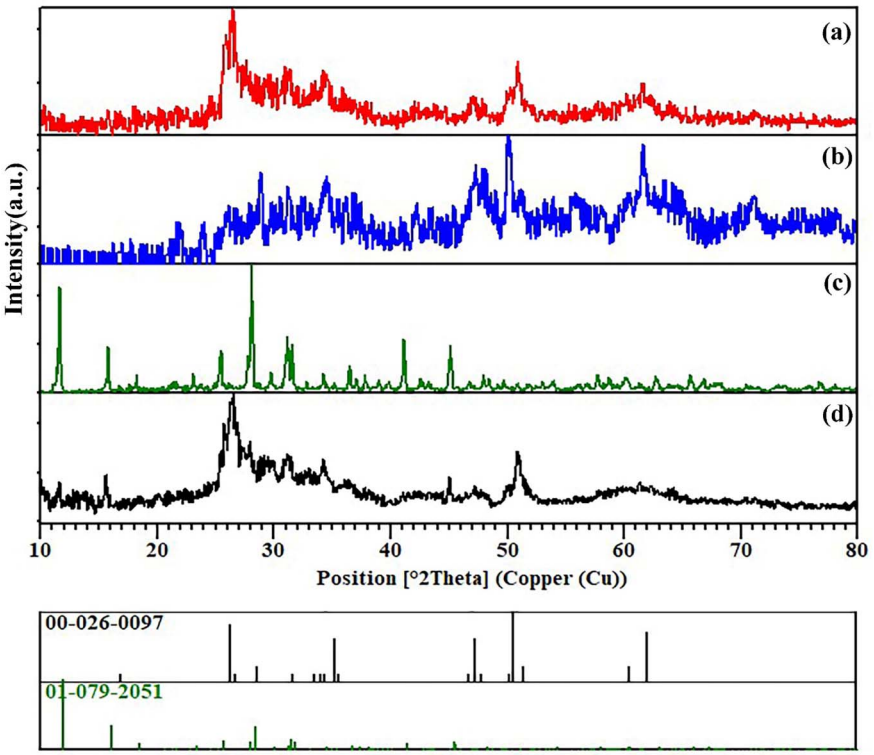

Fig. 1 X-ray diffractogram for samples: (a) NHV0, (b) NHV1, (c) NHV2 and (d) NHV3.

pressure because of the heating procedure. The experiment demonstrated that solvents with different boiling points lead to different internal pressures and morphologies.[34] During the solvothermal process, solvents with higher boiling points generally evaporate at a slower rate, enabling an extended reaction period and promoting the formation of specific structures. In contrast, solvents with lower boiling points evaporate more quickly, resulting in a faster reaction time.[35]

Alcoholic solvents, rather than water, can encapsulate nuclei and influence growth in particular directions while also

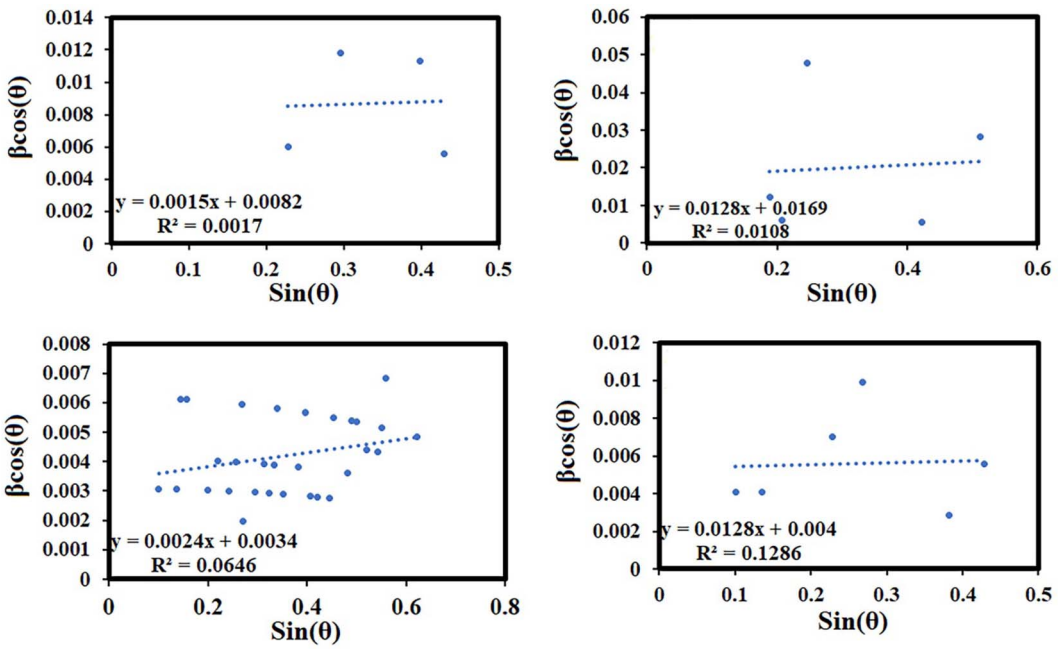

Fig. 2 Derived Williamson–Hall plot from X-ray diffractograms of samples: (a) NHV0, (b) NHV1, (c) NHV2 and (d) NHV3.

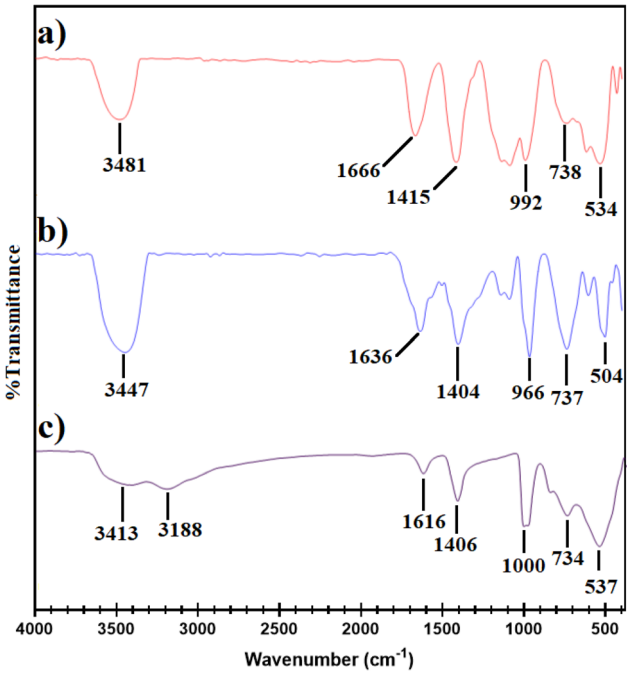

Fig. 3 (a) FT-IR spectra of samples: (a) NHV1, (b) NHV2 and (c) NHV3.

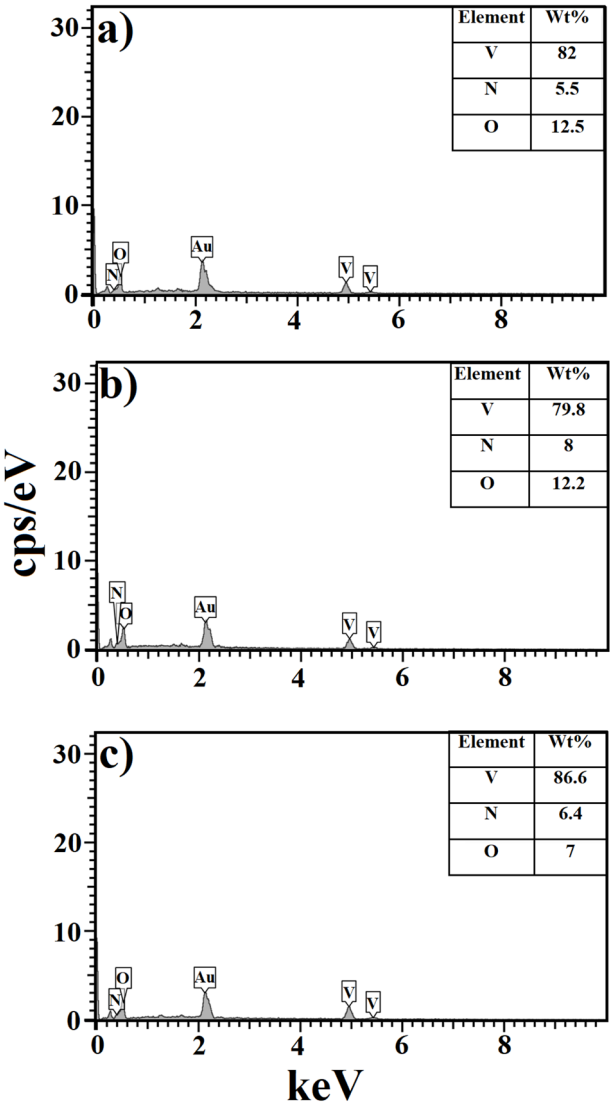

Fig. 4 (a) EDS analysis of samples: (a) NHV1, (b) NHV2 and (c) NHV3.

reducing agglomeration due to the presence of carbon chains. Longer carbon chains provide more extensive coverage but tend to promote agglomeration. In contrast, solvents with shorter carbon chains can distribute themselves among the formed crystals, fostering uniform growth along a defined direction.[36] Polar solvents such as water and alcohol play a crucial role in stabilizing nanoparticle surfaces, enabling the synthesis of nanomaterials with controlled shapes and sizes. When nanostructures are dispersed in water, a layer of water molecules surrounds their surface, acting as a stabilizing barrier to prevent aggregation. Moreover, the polarity of the solvent can affect the binding energy between the participating atoms or molecules, thereby influencing the crystal structure and morphology of the resulting nanomaterials[37,38]

To specify the surface area, porosity and pore volume of the fabricated $(NH_4)_2V_{10}O_{25}\cdot 8H_2O$, the BET-BJH technique was applied, as shown in Fig. 7. The N_2 adsorption–desorption isotherm is related to IV type (H3 category) based on IUPAC sorting.[39] This recommends the structures constructions comprising mesopores and slit pores with a non-uniform distribution of size. The apparent surface area is 23.571 m^2 g^{-1} and the total pore volume is 0.04789 cm^3 g^{-1}. The average pore diameter was 8.1269 nm. The inset plot is related to the BJH method and the size distribution of pores in the range of 1–12 nm.

3.2. Electrochemical characterization

The electrochemical features and capacity of fabricated ammonium vanadate samples were estimated from the charge and discharge paths at a constant current of 1 mA after 15 cycles. By carefully considering the curves, the storage capacity for NHV2 (Fig. 8a) and NHV3 (Fig. 7b) samples was determined as 324 and 956 mA h g^{-1}, respectively. Therefore, the optimal sample $(NH_4)_2V_{10}O_{25}\cdot 8H_2O$ nanorods (NHV3) exhibits a maximum capacity of 5268 mA h g^{-1} in the 7th cycle, which fades in the 15th cycle (956 mA h g^{-1}). Overall, the features of the $(NH_4)_2V_{10}O_{25}\cdot 8H_2O$ sample can be advantageous for hydrogen storage as it delivers more active sites for hydrogen adsorption to the surface of the material.

Cyclic voltammograms for samples NHV2 and NHV3 with different purity of $(NH_4)_2V_6O_{16}$ and $(NH_4)_2V_{10}O_{25}\cdot 8H_2O$ were estimated to examine the electrochemical action in 2.0 M KOH electrolyte solution with a scan rate of 0.1 mV s^{-1} through a usual set of three electrodes. Cyclic voltammetry for the NHV3 sample showed higher anodic and cathodic currents (corresponding to hydrogen absorption and desorption, respectively) than the NHV2 sample (Fig. 8c). The cathodic current and potential for NHV2 and NHV3 are (−0.438 μA, 6869 V) and (−0.426 μA, 9024 V), respectively. The anodic data for NHV2 and

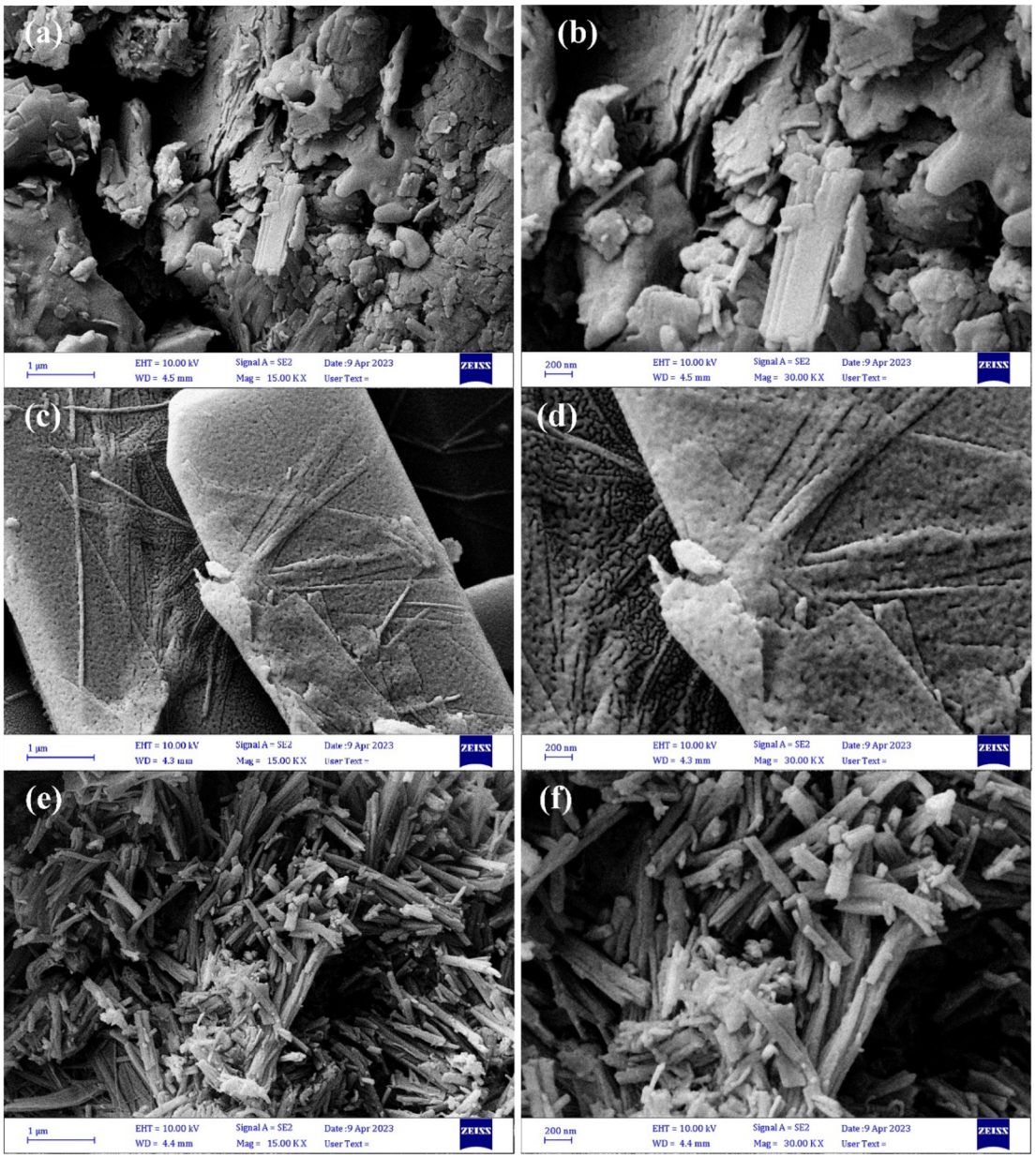

Fig. 5 FE-SEM images for sa ples (a and b) NHV1, (c and d) NHV2 and (e and f) NHV3.

NHV3 are (−0.680, −4518 V) and (−0.694, −8947 V), respectively. In other words, the $(NH_4)_2V_{10}O_{25}\cdot 8H_2O$ nanorods are suitable electroactive materials for energy storage applications.

According to the redox mechanism, the developed electrode materials contain vanadium with oxidation states of +5 and +4, which can undergo reduction to valence. During the ion intercalation process, the electrical neutrality of the oxides is preserved by reducing the high-valence vanadium ion to a low-valence vanadium ion. The existing body of literature suggests that vanadium is reduced, and the redox couple of vanadium is believed to have a significant impact on hydrogen sorption. The vanadium oxide construction successfully achieved charge equilibrium through the process of hydrogen sorption. In the presence of hydrogen, the vanadate molecule exhibits a propensity for hydrogen bonding, leading to the formation of hydroxyl ions. The transformation of the central metal (vanadium) from its high-oxidation state (IV or V) to its low-oxidation state (II) is also included in the previously described process.[40]

In electrochemical energy storage systems, the nanostructure morphology can be adjusted to increase the energy and charge densities. The nanoarchitecture can also be tuned for improvement. In this context, nanostructure materials have rapidly progressed toward 1D nanoparticle assembly. Some researchers have synthesized 1D nanostructures to improve ion diffusivity and electron conductivity. 1D nanostructures enable ions to diffuse through the lattice faster from the core to the surface, resulting in superior electrochemical performance and capacity retention. This led researchers to create novel 1D

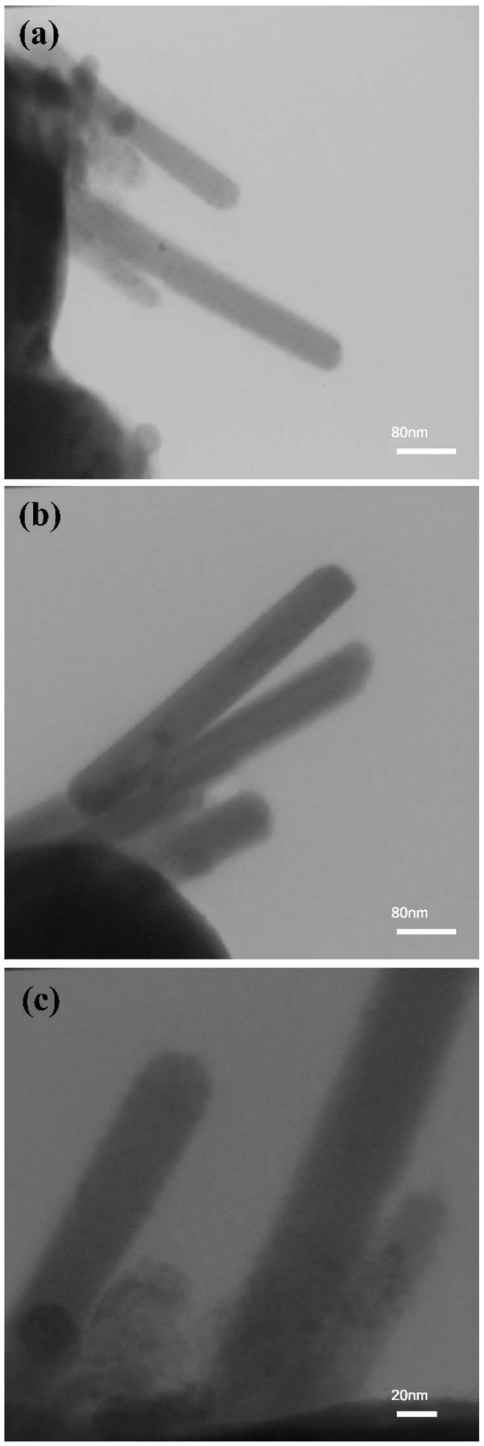

Fig. 6 TEM images for sample NHV3 in different magnifica–ions (a–c).

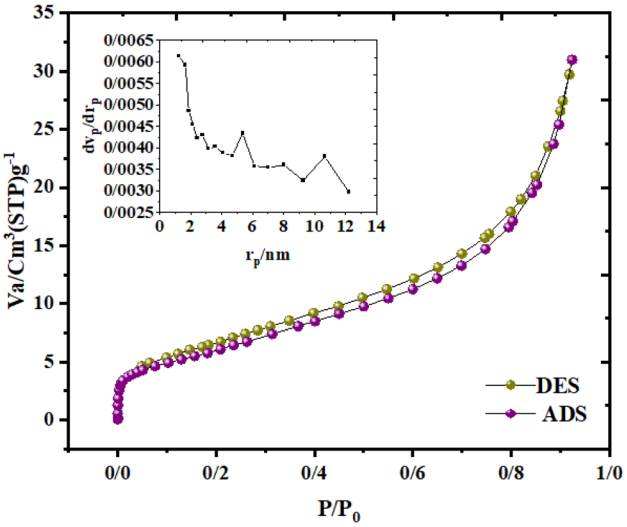

Fig. 7 BET isotherms and BJH plot for the sample NHV3.

nanostructures with unique mechanical, thermal, electrical, and structural features that could improve electrochemical energy storage systems. Scientists have attempted to fabricate nanotubes, nanorods, nanobelts, and nanoribbons. Nanosheets, nanoribbons, and nanoplates may improve electrochemical performance by increasing surface area and reducing ion transport paths. Nanoribbon electrodes with tiny diameters and thicknesses have increased hydrogen storage capacity owing to quick surface charge transfer and better ion diffusion.[41,42]

The physisorption process and the redox method are two possible mechanisms of hydrogen storage. The newly formed H^+ ions stick to the electrode material when a positive electric current is applied (charge moving in the positive direction). The reformation of H_2O occurs when the working electrodes are subjected to an oppositely applied negative current (discharge), which causes the hydrogen molecules contained there to migrate away. The process was conducted using a physisorption mechanism.[43]

Electrochemical processes provide one way to understand adsorption-based storage. At the working electrode, water is used as a proton source in the electrolyte solution, which causes an electron reaction that produces OH^-. The created hydrogen is either adsorbed onto the adsorbent's surface (NHV) according to eqn (2), or it may recombine to form molecules of hydrogen gas according to eqn (3)–(5).

$$H_2O + e^- \rightarrow H_{ads} + OH^- \quad (1)$$

$$NHV + H \rightarrow NHVH_{ads} \quad (2)$$

$$NHVH_{ads} + H_2O + e^- \rightarrow H_2 + OH^- + NHV \quad (3)$$

$$2H \rightarrow H_2 \quad (4)$$

$$NHVH_{ads} + NHVH_{ads} \rightarrow H_2 + 2NHV \quad (5)$$

At various points in the electrochemical process, the Volmer, Heyrovsky, and Tafel reactions are reflected in eqn (1), (3) and (4), respectively. Through an electrochemical process, molecular hydrogen is formed when hydrogen atoms recombine. This occurs when the activation barrier for either the Tafel or Heyrovsky reactions is sufficiently low, and the energy released from the hydrogen adsorption process is less than the energy created during the reaction. The adsorbed hydrogen may end up in

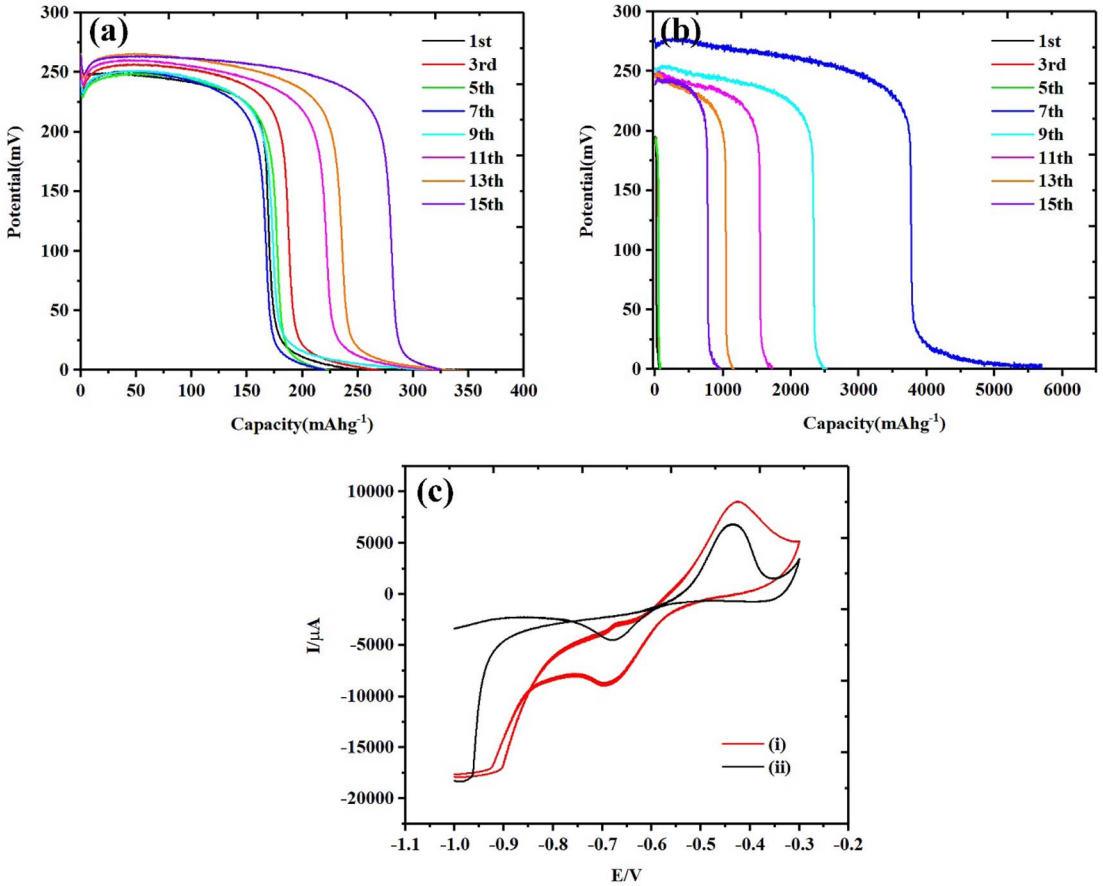

Fig. 8 Voltage plotting versus discharge capacity for samples (a) NHV2, (b) NHV3 and (c) cyclic voltammograms for (i) NHV3 and (ii) NHV2.

more energy-intensive spots in the adsorbent if this does not happen.[44]

4. Conclusion

The solvothermal method was used to produce electrode materials with custom-made ID nanorod shapes. Samples with varied morphologies and compositions were obtained because of various environmental factors. Using the chemical formulas $(NH_4)_2V_6O_{16}$ and $(NH_4)_2V_{10}O_{25}\cdot 8H_2O$. To compare the activity of electrode materials with varying phase purities, the charge–discharge test was performed. After 15 cycles at 1 mA current density, the $(NH_4)_2V_{10}O_{25}\cdot 8H_2O$ that was manufactured showed a capacity of 956 mA h g^{-1}, and the highest capacity was 5268 mA h g^{-1} during the 7th cycle. On the other hand, the capacity of the $(NH_4)_2V_6O_{16}$ electrode material is 324 mA h g^{-1}. Hydrogen storage efficiency in electrodes may therefore be enhanced by the use of 1D structural design because of the poor conductivity of vanadium oxide-based materials.

Data availability

The authors confirm that the data supporting the findings of this study are available within the article. Additional data are available from the corresponding author upon reasonable request.

Conflicts of interest

The authors declare that there are no conflicts of interest regarding the publication of this manuscript.

Acknowledgements

The authors appreciate the University of Kashan for financing this research by grant no. 1392548 and 159271/FS7 and Iran National Science Foundation (INSF) (4032427). Authors would like to thank Miss Angham Husseini (SAMA Research Center) for her valuable help in making and supporting SAMA 500 Electroanalyzer instrument.

References

1 P. R. Prabhukhot, M. Wagh Mahesh and C. Gangal Aneesh, A review on solid state hydrogen storage material, *Adv. Energy Power*, 2016, **4**, 11–22.
2 T. Abbasi and S. Abbasi, 'Renewable' hydrogen: prospects and challenges, *Renewable Sustainable Energy Rev.*, 2011, **15**, 3034–3040.

3 A. Midilli, M. Ay, I. Dincer and M. Rosen, On hydrogen and hydrogen energy strategies II: future projections affecting global stability and unrest, *Renewable Sustainable Energy Rev.*, 2005, **9**, 273–287.
4 E. Rivard, M. Trudeau and K. Zaghib, Hydrogen storage for mobility: a review, *Materials*, 2019, **12**, 1973.
5 F. Dawood, M. Anda and G. Shafiullah, Hydrogen production for energy: an overview, *Int. J. Hydrogen Energy*, 2020, **45**, 3847–3869.
6 A. Züttel, A. Borgschulte and L. Schlapbach, *Hydrogen as a Future Energy Carrier*, 2008.
7 P. Denholm, G. L. Kulcinski and T. Holloway, Emissions and energy efficiency assessment of baseload wind energy systems, *Environ. Sci. Technol.*, 2005, **39**, 1903–1911.
8 D. Gust, T. A. Moore and A. L. Moore, Solar fuels via artificial photosynthesis, *Acc. Chem. Res.*, 2009, **42**, 1890–1898.
9 E. Barbier, Nature and technology of geothermal energy: a review, *Renewable Sustainable Energy Rev.*, 1997, **1**, 1–69.
10 M. Appl, *Ammonia: Priciples & industrial practice*, 1999.
11 S. E. Hosseini and M. A. Wahid, Development of biogas combustion in combined heat and power generation, *Renewable Sustainable Energy Rev.*, 2014, **40**, 868–875.
12 M. Gardiner and S. Satyapal, Energy requirements for hydrogen gas compression and liquefaction as related to vehicle storage needs, *DOE Hydrogen and Fuel Cells Program Record*. 2009, p. 9013.
13 A. Eftekhari and B. Fang, Electrochemical hydrogen storage: opportunities for fuel storage, batteries, fuel cells, and supercapacitors, *Int. J. Hydrogen Energy*, 2017, **42**, 25143–25165.
14 J. Ren, N. M. Musyoka, H. W. Langmi, M. Mathe and S. Liao, Current research trends and perspectives on materials-based hydrogen storage solutions: a critical review, *Int. J. Hydrogen Energy*, 2017, **42**, 289–311.
15 W. Chen, Y. Zhu, C. Yang, J. Zhang, M. Li and L. Li, Significantly improved electrochemical hydrogen storage properties of magnesium nickel hydride modified with nano-nickel, *J. Power Sources*, 2015, **280**, 132–140.
16 W. Zhang, C. Zuo, C. Tang, W. Tang, B. Lan, X. Fu, *et al.*, The current developments and perspectives of V_2O_5 as cathode for rechargeable aqueous zinc-ion batteries, *Energy Technol.*, 2021, **9**, 2000789.
17 H. Chen, H. Qin, L. Chen, J. Wu and Z. Yang, V_2O_5@ CNTs as cathode of aqueous zinc ion battery with high rate and high stability, *J. Alloys Compd.*, 2020, **842**, 155912.
18 J. Hu, H. Chen, K. Xiang, L. Xiao, W. Chen, H. Liao, *et al.*, Preparation for V_6O_{13}@ hollow carbon microspheres and their remarkable electrochemical performance for aqueous zinc-ion batteries, *J. Alloys Compd.*, 2021, **856**, 157085.
19 D. Kundu, S. H. Vajargah, L. Wan, B. Adams, D. Prendergast and L. F. Nazar, Aqueous *vs.* nonaqueous Zn-ion batteries: consequences of the desolvation penalty at the interface, *Energy Environ. Sci.*, 2018, **11**, 881–892.
20 Y. Liu, Z. Pan, D. Tian, T. Hu, H. Jiang, J. Yang, *et al.*, Employing "one for two" strategy to design polyaniline-intercalated hydrated vanadium oxide with expanded interlayer spacing for high-performance aqueous zinc-ion batteries, *Chem. Eng. J.*, 2020, **399**, 125842.
21 J. Tian, L. Yang, L. Zha, R. Wang, S. Huang, G. Xu, *et al.*, Heterostructured multi-yolk-shell SnO_2/Mn_2SnO_4@C nanoboxes for stable and highly efficient Li/Na storage, *J. Power Sources*, 2021, **506**, 230243.
22 H. Jiang, Y. Zhang, Z. Pan, L. Xu, J. Zheng, Z. Gao, *et al.*, Facile hydrothermal synthesis and electrochemical properties of $(NH_4)_2V_{10}O_{25}\cdot 8H_2O$ nanobelts for high-performance aqueous zinc ion batteries, *Electrochim. Acta*, 2020, **332**, 135506.
23 Y. Jiang, L. Jiang, Z. Wu, P. Yang, H. Zhang, Z. Pan, *et al.*, *In situ* growth of $(NH_4)_2V_{10}O_{25}\cdot 8H_2O$ urchin-like hierarchical arrays as superior electrodes for all-solid-state supercapacitors, *J. Mater. Chem. A*, 2018, **6**, 16308–16315.
24 T. Wei, Q. Li, G. Yang and C. Wang, Highly reversible and long-life cycling aqueous zinc-ion battery based on ultrathin $(NH_4)_2V_{10}O_{25}\cdot 8H_2O$ nanobelts, *J. Mater. Chem. A*, 2018, **6**(41), 20402–20410.
25 J. Wang, Y. Zhang, F. Qiao, Y. Jiang, R. Yu, J. Li, *et al.*, Freestanding Ammonium Vanadate Composite Cathodes with Lattice Self-Regulation and Ion Exchange for Long-Lasting Ca-Ion Batteries, *Adv. Mater.*, 2024, **36**, 2403371.
26 W. Wang, W. Wang, F. Xiong, J. Meng, J. Wu, W. Yang, *et al.*, Coupling Manipulation of Interfacial Chemistry and Coordination Structure in Vanadium Oxides Enables Rapid Magnesium Ion Diffusion Kinetics, *Angew. Chem., Int. Ed.*, 2025, **64**, e202414119.
27 P. Gomrokchi, M. Shabani-Nooshabadi, M. Ghiyasiyan-Arani and M. Salavati-Niasari, Tube-on-rod structure of MWCNTs-ammonium cobalt vanadium oxide/ammonium vanadium oxide; evaluation of electrochemical hydrogen storage capacity, *J. Energy Storage*, 2024, **85**, 111041.
28 P. Visakh and M. J. M. Morlanes, *Nanomaterials and Nanocomposites: Zero-To Three-Dimensional Materials and Their Composites*, John Wiley & Sons, 2016.
29 T. Gholami and M. Pirsaheb, Review on effective parameters in electrochemical hydrogen storage, *Int. J. Hydrogen Energy*, 2021, **46**, 783–795.
30 Q. Yang, N. Deng, Y. Zhao, L. Gao, B. Cheng and W. Kang, A review on 1D materials for all-solid-state lithium-ion batteries and all-solid-state lithium-sulfur batteries, *Chem. Eng. J.*, 2023, **451**, 138532.
31 A. Moretti and S. Passerini, Bilayered nanostructured $V_2O_5\cdot nH_2O$ for metal batteries, *Adv. Energy Mater.*, 2016, **6**, 1600868.
32 J. Zheng, Y. Zhang, T. Hu, T. Lv and C. Meng, New strategy for the morphology-controlled synthesis of V_2O_5 microcrystals with enhanced capacitance as battery-type supercapacitor electrodes, *Cryst. Growth Des.*, 2018, **18**, 5365–5376.
33 J. Cao, D. Zhang, Y. Yue, X. Wang, T. Pakornchote, T. Bovornratanaraks, *et al.*, Oxygen defect enriched $(NH_4)_2V_{10}O_{25}\cdot 8H_2O$ nanosheets for superior aqueous zinc-ion batteries, *Nano Energy*, 2021, **84**, 105876.

34 Y.-C. Wu and Y.-C. Tai, Effects of alcohol solvents on anatase TiO_2 nanocrystals prepared by microwave-assisted solvothermal method, *J. Nanopart. Res.*, 2013, **15**, 1–11.
35 T. Gholami, H. Seifi, E. A. Dawi, M. Pirsaheb, S. Seifi, A. M. Aljeboree, *et al.*, A review on investigating the effect of solvent on the synthesis, morphology, shape and size of nanostructures, *J. Mater. Sci. Eng. B*, 2024, **304**, 117370.
36 B. Sinha, R. H. Müller and J. P. Möschwitzer, Bottom-up approaches for preparing drug nanocrystals: formulations and factors affecting particle size, *Int. J. Pharm.*, 2013, **453**, 126–141.
37 S. Gyergyek, D. Makovec and M. Drofenik, Colloidal stability of oleic- and ricinoleic-acid-coated magnetic nanoparticles in organic solvents, *J. Colloid Interface Sci.*, 2011, **354**, 498–505.
38 J.-P. Jolivet, S. Cassaignon, C. Chanéac, D. Chiche, O. Durupthy and D. Portehault, Design of metal oxide nanoparticles: control of size, shape, crystalline structure and functionalization by aqueous chemistry, *C. R. Chim.*, 2010, **13**, 40–51.
39 F. Sedighi, M. Ghiyasiyan-Arani and M. Behpour, $Al_2(WO_4)_3$/$SrWO_4$ electrode modified by date kernel-derived carbon for electrochemical hydrogen storage, *J. Energy Storage*, 2025, **106**, 114883.
40 F. Sedighi, M. Ghiyasiyan-Arani and M. Behpour, Ternary nanocomposites of $Ce_2W_2O_9$/$CoWO_4$/porous carbon; design, structural study and electrochemical hydrogen storage application, *Fuel*, 2022, **310**, 122218.
41 J. N. Tiwari, R. N. Tiwari and K. S. Kim, Zero-dimensional, one-dimensional, two-dimensional and three-dimensional nanostructured materials for advanced electrochemical energy devices, *Prog. Mater. Sci.*, 2012, **57**, 724–803.
42 J. Zheng, Y. Wu, Y. Sun, J. Rong, H. Li and L. Niu, Advanced Anode Materials of Potassium Ion Batteries: from Zero Dimension to Three Dimensions, *Nano-Micro Lett.*, 2020, **13**, 12.
43 M. Ghiyasiyan-Arani, Chapter 4 – Mixed metal oxide-based nanomaterials for hydrogen storage, in: *Renewable and Clean Energy Systems Based on Advanced Nanomaterials*, ed. Zinatloo-Ajabshir S. and Mohammadzadeh A., Elsevier, 2024. pp. 69–97.
44 F. Samimi, M. Ghiyasiyan-Arani, E. A. Dawi and M. Salavati-Niasari, Carbonous nanocomposites of Mn2Mo3O8/MnO as active materials for studying lithium and hydrogen storage application, *J. Energy Storage*, 2024, **75**, 109670.